

Provided for non-commercial research and education use.
Not for reproduction, distribution or commercial use.



This article appeared in a journal published by Elsevier. The attached copy is furnished to the author for internal non-commercial research and education use, including for instruction at the authors institution and sharing with colleagues.

Other uses, including reproduction and distribution, or selling or licensing copies, or posting to personal, institutional or third party websites are prohibited.

In most cases authors are permitted to post their version of the article (e.g. in Word or Tex form) to their personal website or institutional repository. Authors requiring further information regarding Elsevier's archiving and manuscript policies are encouraged to visit:

<http://www.elsevier.com/copyright>



Contents lists available at ScienceDirect

Surface & Coatings Technology

journal homepage: www.elsevier.com/locate/surfcoat

Improved corrosion resistance of AA2024 alloys through hybrid organic–inorganic sol–gel coatings produced from sols with controlled polymerisation

N.C. Rosero-Navarro, S.A. Pellice¹, Y. Castro^{*}, M. Aparicio, A. Durán

Instituto de Cerámica y Vidrio (CSIC), Campus de Cantoblanco, 28049 Madrid, Spain

ARTICLE INFO

Article history:

Received 5 September 2008
Accepted in revised form 13 January 2009
Available online 23 January 2009

Keywords:

Hybrid silica-methacrylate
Sol–gel coatings
Colloidal silica nanoparticles
Aluminium AA2024
Corrosion

ABSTRACT

In this work we present the development of a nanocomposite material composed by silica nanoparticles in a hybrid organic–inorganic sol–gel matrix for corrosion protection of aluminium alloys. The sol–gel matrix was produced from an inorganic precursor, tetraethoxysilane (TEOS), a hybrid precursor organically functionalized with C=C groups, 3-methacryloxypropyltrimethoxysilane (MPS), and an organic bi-functional monomer, ethyleneglycol-dimethacrylate (EGDMA) used to increase the cross-linking network. Silica nanoparticles, on the other side, increase the density and provide a major mechanical performance through the reinforcement of the coating. The evolution of the sol, mainly the chemical structure, during the processes of hydrolytic condensation and organic polymerisation was studied as a function of the sol concentration through Fourier transformed infrared spectroscopy (FTIR), rheometry, laser diffraction analysis and contact angle. Mono and multilayer coatings were deposited by dipping onto AA 2024 substrates and characterised by profilometry. The corrosion behaviour was followed through potentiodynamic tests and Electrochemical Impedance Spectroscopy (EIS).

© 2009 Elsevier B.V. All rights reserved.

1. Introduction

In recent years new sol–gel coatings with rising density and thickness, and improved mechanical behaviour are under development. Those properties are closely related with the performance of coatings in several applications such as corrosion protection [1,2], superficial hardening and optical devices. In many cases the substrates are temperature-sensitive materials as polymers or metallic alloys which could undergo changes of shape or precipitation of second phases during the thermal treatment of coatings, which imposes strong restrictions in coating formulations preventing the use of purely inorganic ones. One important alloy is the AA2024 aluminium alloy commonly used in aircraft industry and defense applications. The anticorrosive protection of this alloy requires high quality standards. At present, the most efficient protection systems are chromate-containing coatings [3], like Chromate Conversion Coatings (CCC) and Chromate Acid Anodised (CAA), which offer a self-healing protection. However, this kind of coatings present high toxicity being dangerous and harmful for health [4]. This was the main reason of European Community to forbid the use of these coatings in all industrial sectors.

Recent works in the field of corrosion protection propose hybrid organic–inorganic sol–gel coatings with interpenetrated networks as

possible substitutes of chromate coatings [5–9]. These films exhibit major possibilities of tailoring properties to fulfil the requirements without affecting the integrity of substrates [10,11]. The organic component provides ductility and facilitates the stress relaxation in the inorganic network; thus, it allows obtaining a drastic increase in thickness without cracking or debonding of coatings [12]. On the other hand, an excess of organic content or a poorly developed organic network could produce a degradation of the mechanical performance. In this sense, it is important to ensure a high cross-linking in both organic and inorganic networks by forming a hybrid material at molecular level. However, the low maximum sintering temperature permitted for this alloy (120 °C), are not enough to produce total densification of the film. One possibility for increasing the density and providing a better mechanical performance is the addition of silica colloidal particles, typically 10–20 nm in size, to the hybrid sol [13].

In this paper we present the description and characterisation of the synthesis of a hybrid organic–inorganic sol reinforced with silica nanoparticles, and the protective barrier effect provided by the hybrid coatings obtained. The matrix of the coatings is constituted by interpenetrated and covalently bonded organic and inorganic networks, a Class II hybrid material according to the classification of Sanchez and Ribot [14]. The silica network was build up from the hydrolytic condensation of tetraethoxysilane (TEOS) and 3-methacryloxypropyltrimethoxysilane (MPS), which has a free-radical polymerisable C=C double bond. A bifunctional monomer, with two C=C double bonds, ethyleneglycol-dimethacrylate (EGDMA), was used to develop a highly crosslinked organic network attached to the inorganic one through covalent Si–C bonds. Organic polymerisation was started in

^{*} Corresponding author. Kelsen, 5, Campus de Cantoblanco, 28049 Madrid, Spain. Tel.: +34 917355840; fax: +34 917355843.

E-mail address: castro@icv.csic.es (Y. Castro).

¹ Current address: Instituto de Investigación en Ciencia y Tecnología de Materiales CONICET, Av. J.B. Justo 4302, B7608FDQ Mar del Plata, Argentina.

liquid state after the hydrolysis of Si–OR groups of TEOS and MPS and colloidal silica addition as a complementary way to increase the final density of the coatings.

The coatings, deposited by dipping onto AA2024 alloy were electrochemically characterised by polarization tests and EIS to determine their efficiency as corrosion barriers against electrolytic attack.

2. Experimental procedure

A series of hybrid organic–inorganic sols was prepared from tetraethoxysilane (TEOS, ABCR 98%), 3-(methacryloxypropyl)trimethoxysilane (MPS, ABCR 98%), ethyleneglycol-dimethacrylate (EGDMA) and a colloidal silica suspension (LUDOX AS-40, aqueous suspension 40 wt.%, particle size 5 nm, pH 9); 2,2'-Azobis (isobutyronitrile) (AIBN, Aldrich, 98%) was used as initiator of the free-radical organic polymerisation. The so called TME-SiO₂ sols were prepared keeping the molar ratio TEOS/MPS/EGDMA of 62.5/25/12.5 and adding the colloidal silica suspension at a 35 mol% respect to alkoxides.

Hydrolytic condensation was catalysed at room temperature with HNO₃ concentrated at a 0.6 vol.% attaining a final pH between 2 and 3. Samples were kept at 4 °C and protected from the light in amber bottles. After this first step of synthesis, the sol has a silica concentration of 4.8 M and a C=C double bonds concentration of 1.78 M. In the second step of synthesis the sol was diluted with absolute ethanol at different concentrations down to a 20 vol.% and exposed to a process of free radical polymerisation of C=C through a thermal decomposition of AIBN at 65 °C in a thermostatic oil bath.

A Fourier Transformed Infrared spectrometer equipped with an Attenuated Total Reflectance accessory (ATR-FTIR, Perkin Elmer, Spectrum 100) with diamond crystal was used to study the hydrolytic condensation of Si–O–Si bonds during the first step of synthesis and the evolution of the C=C groups during the second step in liquid samples. ATR spectra were recorded between 650 and 4000 cm⁻¹, with a resolution of 2 cm⁻¹. Spectra were deconvoluted by the PeakFit software considering Gaussians and Lorentzian bands. Residual RMS errors were around 0.001. Initial and last stages of first hydrolysis step (1 min and 17 h) were repeated using a KRS5 cell and measuring in transmission mode to confirm that no shift of mode frequencies of the vibrations bands occurs.

The polymerisation degree at the gel point (x_{gel}) as a function of the sol concentration was determined by measuring the area of the FTIR band at 1636 cm⁻¹ corresponding to C=C double bonds taking the C=O bands as references.

The evolution of the viscosity of sols during the second step of synthesis at 65 °C was analysed as a function of time using a rotational rheometer (Haake, RS50, Germany) provided with a cone and a plate fixture (5 mL samples) at a shear rate of 600 s⁻¹. The shear rate was increased from 0 to 600 s⁻¹ in 3 min, kept for 1 min at the maximum rate and decreased again to 0 s⁻¹ in 3 min. The stability of the sols after different polymerisation degree was also studied measuring the evolution of viscosity with time at storage conditions of 5 °C.

The behaviour and size evolution of silica nanoparticles were analysed in a sol diluted at a 33 vol.% during the process of organic polymerisation using a laser diffraction analyser (Zetasizer Nano ZS, Malvern Instruments) with a light source of 633 nm.

Glass slides and aluminium alloy AA 2024 substrates (2.5 × 7 cm²) were dip-coated with different polymerised sols at a withdrawal rate of 20 cm/min. Coatings were dried at room temperature and sintered during 120 min at 120 °C in air with a heating rate of 10 °C/min. Multilayer coatings were obtained using an intermediate treatments of 120 °C, 1 h after the deposition of each layer. The coatings thickness was measured by profilometry (Talystep, UK). Wettability of sols onto aluminium substrates was determined by measuring the contact angle with an Easy Drop Krüss equipment.

Electrochemical tests were conducted at room temperature in 0.05 M NaCl solutions using an electrochemical unit (Gamry FAS2

Femtostat). The analysis of the protected substrates with only sol–gel coatings (without additional painting) is usually performed in more diluted NaCl solutions compared with the standard solution (3.5%) used in industrial tests on complete protection systems (with painting). The objective is to obtain more and better information about the mechanisms involved in the corrosion process of the aluminium substrate protected with these coatings.

A conventional three-electrode cell was used using a saturated calomel reference electrode (SCE, Radiometer Copenhagen), a platinum wire as counter-electrode and the test coupons as the working electrode. Potentiodynamic tests were conducted at a scan rate of 0.0002 V s⁻¹ after 1 h of immersion. Impedance measurements (EIS) were performed at different times of immersion in the electrolyte. The tests started by recording the electrode potential with time. When the corrosion potential remained stable, a sinusoidal ac signal of 5 mV (rms) amplitude at the open circuit potential (OCP) was applied to the electrode over the frequency ranged from 3 · 10⁵ Hz down to 10⁻² Hz. Impedance fitting was performed using Gamry Echem Analyst software.

3. Results and discussion

3.1. Hydrolytic condensation

The synthesis of TME-SiO₂ sol proceeds in a two step process. In the first one, the hydrolytic condensation of alkoxides takes place in presence of EGDMA and the colloidal silica suspension under strongly acid catalysis. This process, fast and highly exothermic, was followed by FTIR through the evolution of the vibration bands of Si–O–R bonds of the alkoxides, and the corresponding bands of ethanol and methanol produced by the hydrolytic condensation of TEOS and MPS respectively. Table 1 shows the main FTIR bands appearing.

Fig. 1 shows the ATR-FTIR spectra of the starting solution TEOS-MPS-EDGMA-SiO_{2coll} (absorbance spectra are multiplied by their corresponding volumetric proportions in the sol), which components are immiscible to each other, the resulting sol after 1 and 12 min of vigorous stirring and after 17 h of storage at 4 °C, along with a powdered sample obtained after treatment of the sol obtained in the first synthesis step at 120 °C for 6 h to produce the complete evaporation of solvents. Quantification of silica condensation is difficult to perform due to overlapping of many bands in the same region of the infrared spectra. In the mixture TEOS/MPS/EGDMA, the band of Si–O–

Table 1
FTIR bands (cm⁻¹) of reagents and products of hydrolytic condensation

Component	Wavenumber (cm ⁻¹)	Assignment
TEOS	1169	δ(CH ₃)
	1102	ν _{as} (C–C + C–O) and δ(COH)
	1075	ν _{as} (Si–O–C)
	961	δ(H ₃ CO) and δ(H ₃ CC)
	787	ν(Si–O + C–O)
MPS	1161	δ(CH ₃)
	1078	ν _{as} (Si–O–C)
	940	=CH ₂ wag
	813	=CH ₂ twist
EGDMA	1144 and 813	ν(C–O)
	940	=CH ₂ wag
Ethanol	1088	ν _{as} (C–C + C–O) and δ(COH)
	1045	δ(CCH ₃) and δ(COH)
	880	ν _s (C–C + C–O)
Methanol	1027	ν(C–O(H))
Si–O–Si	1150, 1200	ν _{as} LO
	1113–1120	ν _{as} TO
	1045, 1080 and 1100	ν _{as} TO
	840	ν _s (Si–O–Si) (not observed)
Non-bridging oxigens	975	ν(Si–OH)
	940–960	ν(Si–OH)
	915	ν(Si–O ⁻)
	790–810	δ _s (Si–O)

From Refs. [15–23].

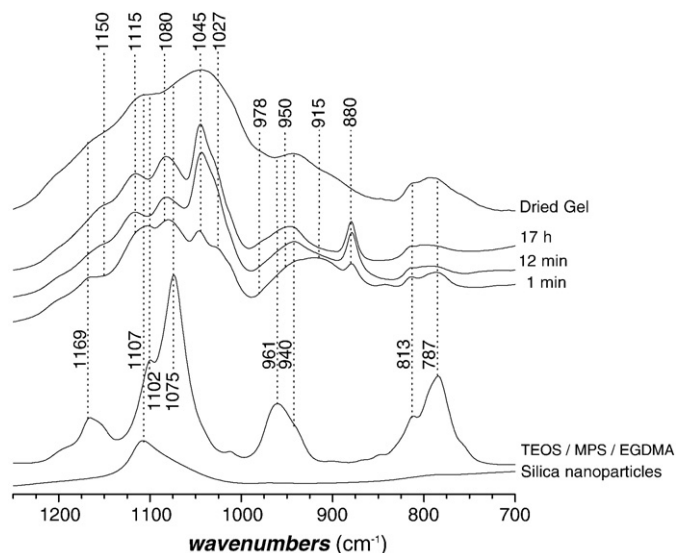


Fig. 1. ATR-FTIR spectra of the starting sol and different stages of hydrolysis of TME-SiO₂ sol after addition of water, along with silica nanoparticles suspension and dried gel.

C bonds of MPS, at 1078 cm⁻¹, are overlapped with the corresponding band of TEOS, at 1075 cm⁻¹, present in higher concentration. Due to similarity of chemical structure of MPS and EGDMA, both compounds present the bands related to the methacryloxy groups at 813 and 940 cm⁻¹ as well as less intense ones at 1161 and 1144 cm⁻¹. Similarly, an important overlapping occurs between bands at 1045 cm⁻¹ corresponding to ethanol and that assigned to Si–O–Si bonds.

After addition of nitric acid to the phase-separated mixture, a spontaneous destabilization of the silica suspension and the initiation of hydrolysis of alkoxides take place simultaneously. Ethanol and methanol bands, produced as a consequence of hydrolysis of TEOS and MPS respectively, are clearly observed after the first minute of synthesis [24]. Although the main bands of Si–O–R groups are overlapped to Si–O–Si ones, the fast hydrolysis of TEOS and MPS is

certainly evidenced by the strong diminution of their bands at lower frequencies, 787 and 813 cm⁻¹.

During the hydrolysis, Si–OH bands at 948 and 978 cm⁻¹ develop [21] and primary silica clusters, evidenced by a strong and broad band of SiO⁻ fragments at 915 cm⁻¹, are produced [25]. These SiO⁻ fragments tend to disappear while primary clusters grow through the advance of the condensation process.

Since hydrolysis and condensation processes take place near simultaneously under acidic conditions, the development of the silica network is observed from the first minute of synthesis. The bands at 1080 cm⁻¹ and 1045 could be assigned to transversal optic (TO) modes of Si–O–Si bonds present, respectively, in cyclic structures like in vitreous silica [26], mainly corresponding to the most energetic bonds in the dense network of colloidal silica, and in smaller siloxane rings with larger Si–O–Si angles and Si–O bond length presents in the sol [20–24,27,28]. The silica band at 1045 cm⁻¹ is near completely developed after 12 min of stirring. The development of a band at 1115 cm⁻¹, attributed to asymmetrical vibration of the Si–O–Si bond in hybrid organic–inorganic sol–gel materials [15,21,22], is also clearly observed. It coincides with the bands observed in the colloidal silica suspension, corresponding to dense silica and situated around 1107 cm⁻¹. On the other hand, although the longitudinal optic (LO) mode is not usually observed in liquid samples, a band at 1150 cm⁻¹ is present in the sol and could so be attributed to the development of more cross-linked structures giving information of the extent of the silica network [29]. Therefore, after 12 min of stirring at 4 °C, hydrolysis has practically finished. The band of methyl and methylene rocking modes of ethanol, at 880 cm⁻¹, reaches its maximum intensity showing only a slight progress after 17 h of storage at 4 °C.

After evaporation of solvents and curing for obtaining dried powders at the end of the synthesis, the sol–gel transformation takes place and the final silica structure can be resolved. In spite of the widening of bands, in the solid state it is possible to distinguish the LO band at 1150 cm⁻¹, being related to the porous structure in the sol–gel matrix [3,30]. TO bands are also present in the solid state at 1080 (sh), 1045 and 1107–1115 cm⁻¹. The shoulder band observed at 1015 cm⁻¹ might be attributed to bending vibration modes of Si–O–Si linkages in cyclosiloxane isolated or terminal rings [28].

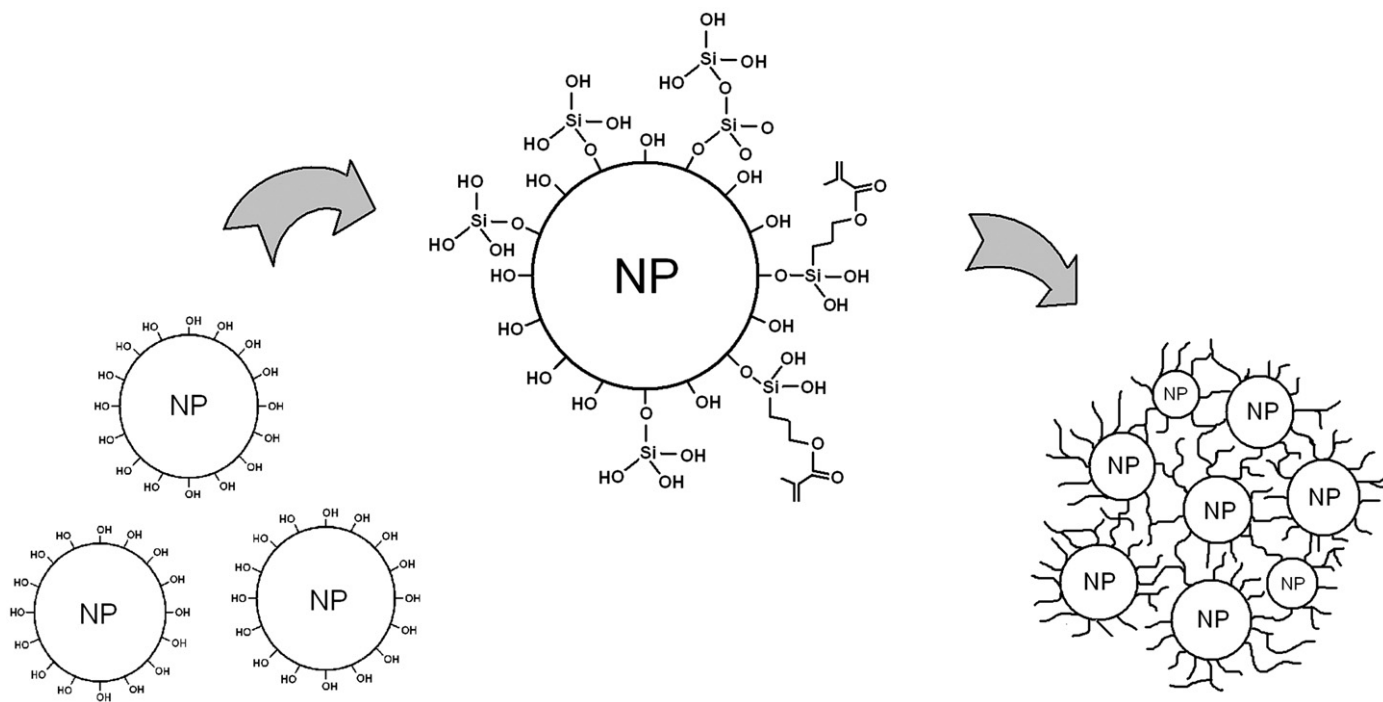


Fig. 2. Schematic representation of grafting and agglomeration of silica nanoparticles (NP) during the process of hydrolytic condensation.

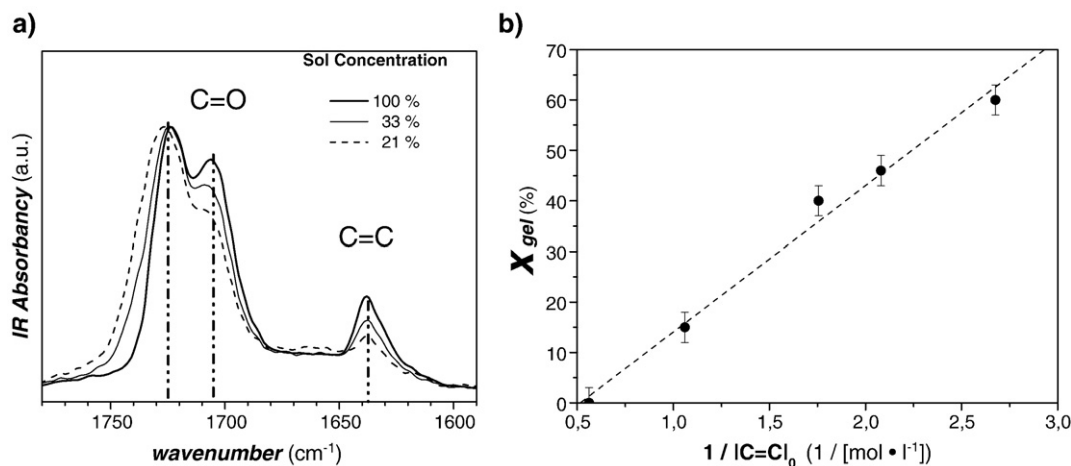


Fig. 3. a) FTIR spectra of TME-SiO₂ and b) polymerisation degree at the gel point as a function of initial C=C concentration.

The process of hydrolytic condensation in the presence of OH-rich silica nanoparticles could produce a modification of the surface (grafting) through covalent bonding to partially hydrolyzed TEOS and MPS. This process could enrich the surface in Si-OH and C=C reactive groups from alkoxides [31,32], Fig. 2. Although the chemical bonding between silica nanoparticles and matrix is very important for increasing density and crosslinking of the coatings, it could also lead to an undesirable agglomeration of nanoparticles. In fact, this phenomenon was observed through laser diffraction analysis. As explained in next point even as the particle size distribution remains in a rather narrow and monomodal curve the particle size grows from 5 to 40 nm at the end of the first step of synthesis.

3.2. Organic polymerisation

During the second step of the synthesis, a free radical polymerisation of the C=C double bonds takes place through the thermal decomposition of AIBN at 65 °C. The key factor that makes possible this process in liquid state without producing an irreversible gelling is the dilution of the sol, leading to the formation of a solution of microgels with a highly crosslinked network [24]. Thus, depending on the amount of solvent, the gel point may change from 0 to 100% of polymerisation of C=C. According to this, the polymerisation process of the TME-SiO₂ sol was analyzed at different concentrations between 20 and 100 vol.%, which correspond to C=C concentrations of 0.38 and 1.78 M respectively.

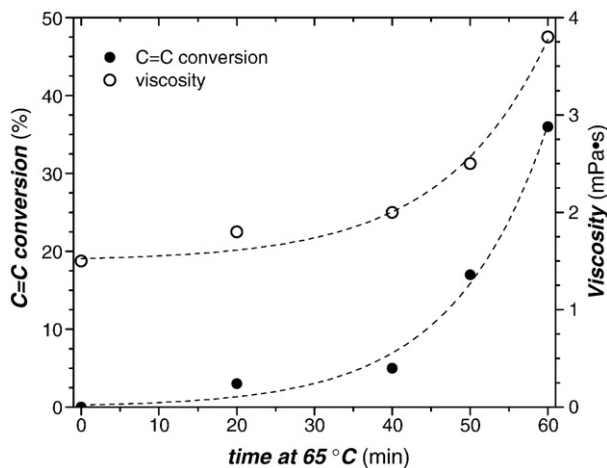


Fig. 4. Evolution of polymerisation of C=C double bonds and viscosity of the sol TME-SiO₂ 30 vol.% during the second step of synthesis at 65 °C.

The decrease in the concentration of C=C groups was followed by ATR-FTIR spectroscopy as a function of sol concentration. Fig. 3a) shows the spectra of sols TME-SiO₂, recorded between 1780 and 1590 cm⁻¹ at gelling time. The lower the sol concentration, the lower is the intensity of the C=C band at 1639 cm⁻¹. The C=O band has three different components [33]: a band at 1705 cm⁻¹ assigned to C=O hydrogen-bonded to OH groups of EGDMA or to Si-OH groups generated in the first stage, a band at 1720 cm⁻¹ assigned to C=O stretching vibrations that are conjugated to C=C double bonds, and a band at 1732 cm⁻¹ assigned to C=O stretching vibrations, produced during the organic polymerisation, and not conjugated to C=C double bonds. The ratio of areas of C=C bands between none polymerised and near gelled samples allows determining the polymerisation degree at gelling time as a function of sol concentration. Fig. 3 shows the experimental data and a fitting curve. The conversion of C=C groups calculated from FTIR spectra at the gel time showed an inversely proportional dependence between x_{gel} and the sol concentration, $x_{gel} \propto 1/[C=C]_0$.

During the second step, the viscosity of sols increases with the organic polymerisation. Fig. 4 shows the close relationship between polymerisation degree and viscosity as a function of the synthesis time at 65 °C in the second step for the sol TME-SiO₂ 30 vol.%.

The advance of polymerisation in the liquid state supposes a great advantage for both deposition process and final cross-linking in the coating. A slight advance in polymerisation of C=C double bonds implicates a cross-linking level enough to allow the deposition of coatings without dropping nor wetting problems. A little evaporation of solvent after deposition produces a fast solidification of the sol leaving to a more consistent and smoother coating when it is produced with a partially polymerised sol.

Since the wettability of the substrates is mainly governed by the solvent, ethanol, the contact angle of the sol TME-SiO₂ 30 vol.% does not change significantly with the polymerisation degree, maintaining around 19° on aluminium AA2024.

During the process of organic polymerisation, the agglomerates of silica nanoparticles formed during the first step (Fig. 2) increase slightly their diameter keeping a still monodisperse but wider size distribution even up to a 20% of C=C conversion bonds. Fig. 5 shows the evolution of the size distribution of silica nanoparticles along the complete two-step process of synthesis for the sol TME-SiO₂ 30 vol.%.

The viscosity increase resulting from the organic polymerisation advance and the size distribution of particles as well has a strong influence on the stability of sols. The presence of large agglomerates with Si-OH enriched surfaces favours the percolation of particles through inorganic condensation processes which accelerate the viscosity rising rate reaching the gelling point at lower times. This parameter is a very relevant factor for application at industrial scale. In

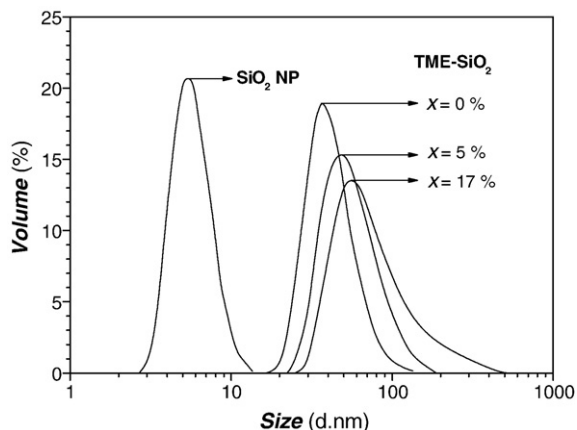


Fig. 5. Size particle distribution of colloidal silica nanoparticles (as received) and sols TME-SiO₂ 30 vol.% with different polymerisation degrees.

dipping process the viscosity, η , of sols is related with the coating thickness, t , as $t \propto \eta^{1/2}$ [34–36]. On the other hand, in spray deposition process, viscosity of sols is usually not higher than 5 mPa s in order to avoid problems with tubes, nozzles or high pressures in equipments. The rheological study of TME-SiO₂ sols evidenced the acceleration of viscosity evolution for increasing polymerisation degrees. Even so, stable sols have been obtained for reliable storage time up to 400 h at 5 °C with the 18% polymerised sol at 30% (Fig. 6), which could be considered a suitable stability for sol–gel sols.

3.3. Characterisation of the coatings

Transparent, colourless and crack-free coatings were obtained using the sol TME-SiO₂ 30 vol.% after the processes of dip-coating and thermal treatment at 120 °C for 2 h. The thickness of the monolayers was 1.1 and 2.1 μm for sols organically polymerised at 18 and 36% respectively. The higher viscosity of the latter sol leads to thicker coatings when the same withdrawal rate is applied. The thickness of multilayer coatings were obtained as addition of single layers, being 3.1 and 6 μm for 18 and 36% polymerised 3-layer coatings respectively.

Potentiodynamic polarization curves, carried out on three-layer coatings after 1 h of immersion in 0.05 M NaCl electrolyte, are shown in Fig. 7 along with bare AA2024 reference. The curve for the aluminium alloy shows a material in active dissolution with no signs of passivity in the studied potential range. The coatings show a significant improvement of corrosion resistance with the presence of a region of potentials of quasi stable current density, $5 \cdot 10^{-10}$ and $2 \cdot 10^{-7}$ A cm⁻² for coatings prepared with 18 and 36% polymerised sols, respectively.

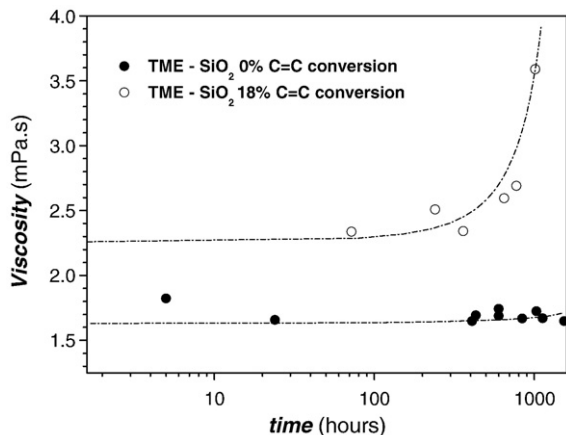


Fig. 6. Evolution of viscosity at 5 °C of the TME-SiO₂ sols 30 vol.% with different polymerisation degrees.

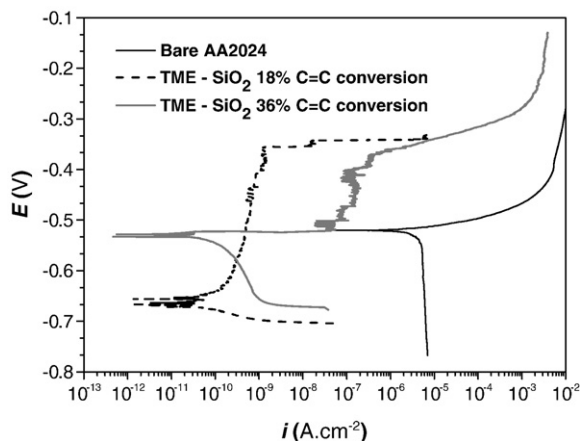


Fig. 7. Potentiodynamic polarization curves after 1 h of immersion on three-layer coatings using 18 and 36% polymerised 30 vol.% sols compared with bare metal substrate.

The potential breakdown of these coatings, -350 mV, indicates that both coatings provide a similar protection. However, the reduction of current density is higher for the less polymerised coating. This effect could indicate a higher homogeneity and integrity of the coatings produced from the 18% polymerised sol. The higher organic polymerised sols usually present a higher density of defects, like pores and microcracks, in the resulting coating, explaining the lower protection behaviour. The presence of silica nanoparticles allows increasing the density as well as a higher network condensation with the improvement

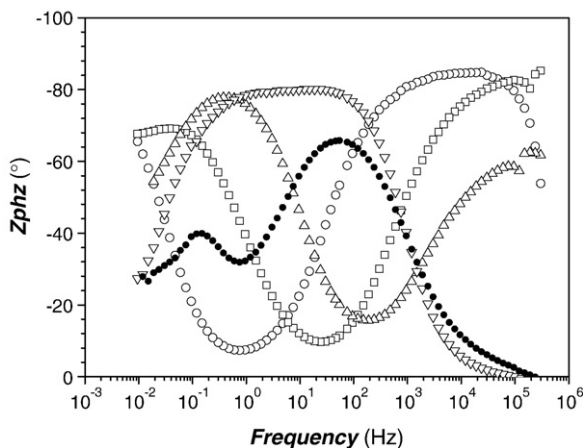
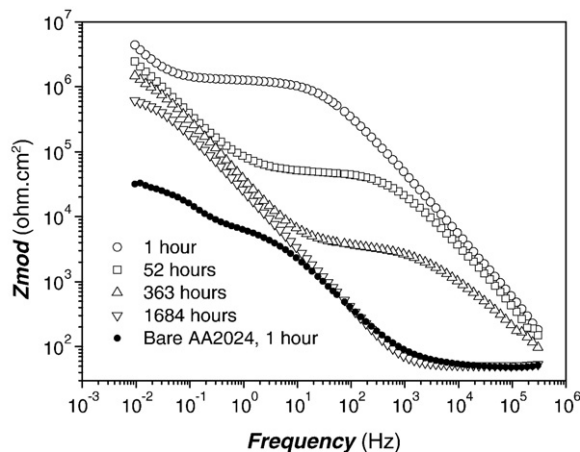


Fig. 8. Bode diagrams after different immersion times of an AA2024 substrate protected with a three-layer coating (3.3 μm) prepared using the 18% polymerised 30 vol.% sol compared with bare metal substrate after 1 h of immersion.

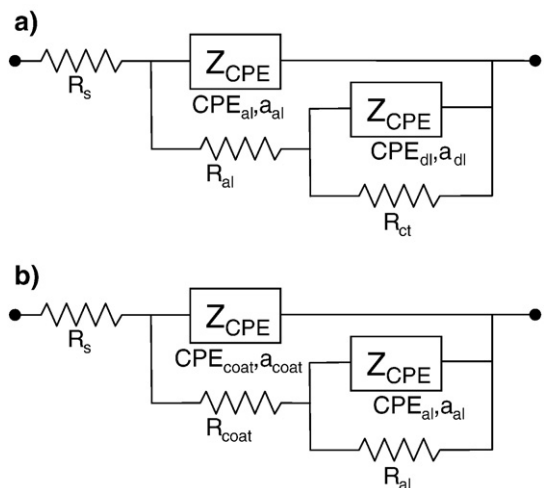


Fig. 9. Equivalent circuits used to fit the EIS spectra: (a) Bare AA2024 after 1 h of immersion and coated substrate after 1684 h; (b) Coated AA2024 substrate after 1, 52 and 363 h.

of the cross-linking. A similar system without silica nanoparticles has shown a very limited corrosion protection because the more open structure of the films [37].

Getting deeper in the electrochemical characterisation, AC impedance was performed for bare substrates and a three-layer coating produced with the 18% polymerised sol (Fig. 8). The phase angle curve of the bare alloy presents two time constants at 55 and 0.15 Hz, assigned to the intermediate aluminium oxide layer and the electron charge transfer process from corrosion, respectively [38,39]. A new time constant at higher frequencies, above 10^4 Hz, associated with the sol-gel coating, appears in the spectra of the protected substrates. The incorporation of this coating produced an increase of impedance modulus at 0.01 Hz of two orders of magnitude as a consequence of the additional barrier provided. Bode plots of coated samples after only 1 h of immersion present two time constants at 10^4 Hz (sol-gel coating) and around 10^{-2} Hz (intermediate layer).

The increase of the immersion time in the electrolyte produced a slow deterioration of the corrosion protection system. The observed plateau between 1 and 1000 Hz, associated with the resistances assigned to the NaCl solution and sol-gel coating, decreases with immersion time and moves to higher frequencies, indicating a coating degradation. The reduction of phase angle of the higher frequency time constant with immersion time indicates a less capacitive response due to permeation of solution through the micropores in the sol-gel coating. After 363 immersion hours, the corrosion process begins to be evident by the presence of two time constants at low frequencies and the disappearing of the time constant associated with the sol-gel coating.

The interpretation of impedance spectra was performed using a numerical fitting. The equivalent circuits used to model all impedance curves are displayed in Fig. 9. In the simulation, the constant phase element (CPE) was used instead of an “ideal” capacitor to explain the deviations from ideal behaviour. The impedance of a CPE (Z_{CPE}) can be defined by $Z_{CPE}=(1/Y)/(j\omega)^a$. The parameters correspond to the frequency (ω), pseudo-capacitance (Y), and the parameter a associated to the system homogeneity. When this equation describes a capacitor, $a=1$ and $Y=C$ (the capacitance). For a CPE, the exponent a is less than one. R_s is the resistance of the electrolyte and R_{coat} the resistance of the sol-gel coating. Y_{coat} is the pseudo-capacitance of the sol-gel coating, and $R_{alumina}$ and $Y_{alumina}$, the resistance and pseudo-capacitance associated with the thin natural aluminium oxide layer. R_{ct} is the resistance describing the corrosion of the metal substrate, and Y_{dl} the double-layer pseudo-capacitance formed in the metal-electrolyte interface. These equivalent circuits are used in several

Table 2
Impedance parameters for bare and coated AA2024 substrates

Time (h)	R_s (ohm cm^2)	R_{coat} (ohm cm^2)	Y_{coat} (S cm^{-2} s a)	a_{coat}	R_{al} (ohm cm^2)	Y_{al} (S cm^{-2} s b)	a_{al}	R_{ct} (ohm cm^2)	Y_{dl} (S cm^{-2} s c)	a_{dl}
Bare, 1	49.80±0.39	—	—	—	6.40E3±2.25E2	1.33E-5±3.81E-7	0.820±4.2E-3	3.78E4±1.62E3	1.05E-4±3.06E-6	0.740±19.3E-3
1	72.10±4.10	1.22E6±9.30E3	6.80E-9±1.26E-10	0.930±1.8E-3	11.15E6±1.29E6	3.43E-6±1.19E-7	0.960±16.3E-3	—	—	—
52	55.00±3.46	4.63E4±3.74E2	1.13E-8±3.59E-10	0.920±2.8E-3	47.44E6±24.29E6	3.94E-6±3.20E-8	0.800±4.8E-3	—	—	—
363	22.77±2.74	3.51E3±37.90	1.70E-7±1.14E-8	0.770±5.8E-3	2.26E6±6.86E4	5.14E-6±4.22E-8	0.880±3.0E-3	—	—	—
1684	51.37±0.47	—	—	—	2.74E3±2.05E3	4.79E-6±6.94E-7	0.970±16.7E-3	7.65E5±1.98E4	3.16E-6±6.79E-7	0.730±26.4E-3

papers [38–41] to fit impedance spectra in the case of aluminium alloys covered with hybrid silica sol–gel coatings. Table 2 shows the fitting of the data for the models presented in Fig. 9.

The R_{coat} reduction and Y_{coat} increasing can be associated with the water uptake through pores and defects in the coating leading to a continuous deterioration of the corrosion protection system. The value of R_{alumina} of the coated substrate after 1 h of immersion is significantly higher than that of the bare substrate, probably due to the infiltration of the alumina layer porosity with the sol during the coating deposition process. This impedance decreases with immersion time showing also the degradation of system. The corrosion after 1684 h of immersion originates a higher value of R_{ct} compared with the bare substrate, indicating the existence of some protection even after this long immersion time.

4. Conclusions

A transparent and homogeneous hybrid organic–inorganic sol containing silica nanoparticles was produced through a process of hydrolytic condensation of Si–O–R groups followed by free-radical organic polymerisation of C=C double bonds in liquid state. During the hydrolytic condensation, silica nanoparticles agglomerate in clusters of around 40 nm which show high stability during the process of organic polymerisation.

The gelling time of sols depends on the C=C double bonds being inversely proportional with the sol concentration; with $x_{\text{gel}}=60\%$ for the sol TME–SiO₂ 20 vol.% and $x_{\text{gel}}=0\%$ for the non-diluted one. The sol diluted at 30% is stable for more than 400 h when stored at 5 °C.

Multilayer sol–gel coatings obtained on AA2024 substrates enhance the corrosion resistance of the alloy showing a barrier effect up to 360 immersion hours. Potentiodynamic polarization curves of coatings produced from 30 vol.% sol polymerised at 36% of C=C indicate the presence of a structure with more defects suggesting the suitability of a maximum polymerisation level for barrier properties.

Acknowledgements

The authors acknowledge the funding provided by the European Community, MULTIPROTECT project: “Advanced environmentally friendly multifunctional corrosion protection by nanotechnology”, Contract No. NMP3-CT-2005-011783, and by the Spanish Ministry of Science and Innovation (project MAT2006-4375). Otherwise the JAE fellowship of Carolina Rosero-Navarro is thanked to CSIC. The authors thank Laura Peláez for her assistance with the experimental techniques.

References

- [1] J.M. Gomez-Vega, A. hozumi, E. Saiz, A.P. Tomsia, H. Sugimura, O. Takai, J. Biomed. Mater. Res. 56 (2001) 382.
- [2] G. Bierwagen, J. Coat. Technol. 73 (2001) 45.
- [3] E. McCafferty, Corros. Sci. 29 (1989) 391.
- [4] U. S. Public Health Service, Repot no. STSDR/TP-88/10 July, 1989.
- [5] M.L. Zheludkevich, M.G.S. Ferreira, I.M. Miranda Salvado, J. Mater. Chem. Rev. 15 (2005) 5099.
- [6] J.H. Osborne, K.Y. blohowiak, S.R. Taylor, C. Hunter, G. Bierwagon, B. Carlson, D. Bernard, M.S. Donley, Prog. Org. Coat. 41 (2001) 217.
- [7] M.L. Zheldukelvich, R. Serra, M.F. Montemor, I.M. Miranda Salvado, M.G.S. Ferreira, Surf. Coat. Technol. 200 (2004) 4040.
- [8] A. Conde, A. Duran, J.J. de Damborenea, Prog. Org. Coat. 46 (2003) 288.
- [9] W.J.V. Ooij, D. Zhu, V. Palanivel, J.A. Lamar, M. Stacy, Silicon Chem. 3 (2006) 11.
- [10] L.Y.L. Wu, E. Chwa, Z. Chen, X.T. Zeng, Thin Solid Films 516 (2008) 1056.
- [11] F. Mammeri, E. Le Bourhis, L. Rozesa, C. Sanchez, J. Mater. Chem. 15 (2005) 3787.
- [12] S. Pellice, P. Galliano, Y. Castro, A. Durán, J. Sol-Gel Sci. Technol. 28 (2003) 81.
- [13] S. Pellice, U. Gilabert, C. Solier, Y. Castro, A. Duran, J. Sol-Gel Sci. Technol. 348 (2004) 172.
- [14] C. Sanchez, F. Ribot, New J. Chem. 18 (1994) 1007.
- [15] P. Innocenzi, G. Brusatin, J. Non-Cryst. Solids 333 (2004) 137.
- [16] P. Innocenzi, J. Non-Cryst. Solids 316 (2003) 309.
- [17] C. Wu, Y. Wu, T. Xu, W. Yang, J. Non-Cryst. Solids 352 (2006) 5642.
- [18] M. Tomozawa, Y.K. Lee, Y.L. Peng, J. Non-Cryst. Solids 242 (1998) 104.
- [19] N. Viart, D. Niznansky, J.L. Rehspringer, J. Sol-Gel Sci. Technol. 8 (1997) 183.
- [20] G. Wu, J. Wang, J. Shen, T. Yang, Q. Zhang, B. Zhou, Z. Deng, B. Fan, D. Zhou, F. Zhang, Mater. Res. Bull. 36 (2001) 2127.
- [21] A. Jitianu, A. Britchi, C. Deleanu, V. Badescu, M. Zaharescu, J. Non-Cryst. Solids 319 (2003) 263.
- [22] C.M. Bertelsen, F.J. Boerio, Prog. Org. Coat. 41 (2001) 239.
- [23] S.K. Medda, D. Kundu, G. De, J. Non-Cryst. Solids 318 (2003) 149.
- [24] S.A. Pellice, R.J.J. Williams, I. Sobrados, J. Sanz, Y. Castro, M. Aparicio, A. Durán, J. Mater. Chem. 16 (2006) 3318.
- [25] A. Chmel, E.K. Mazurina, V.S. Shashkin, J. Non-Cryst. Solids 122 (1990) 285.
- [26] N. Viart, J.L. Rehspringer, J. Non-Cryst. Solids 195 (1996) 223.
- [27] A. Fidalgo, L.M. Ilharco, J. Non-Cryst. Solids 283 (2001) 144.
- [28] Z. Sassi, J.C. Bureau, A. Bakkali, Vib. Spectrosc. 28 (2002) 299.
- [29] N. Primeau, C. Vautey, M. Langlet, Thin Solid Films 310 (1997) 47.
- [30] R.M. Almeida, C.G. Pantano, J. Appl. Phys. 68 (1990) 4225.
- [31] N. Nishiyama, R. Shick, H. Ishida, J. Colloid. Interface Sci. 143 (1991) 146.
- [32] M.W. Daniels, L.F. Francis, J. Colloid Interface Sci. 205 (1998) 191.
- [33] P. Innocenzi, G. Brusatin, S. Licocchia, M.L. Di Vona, F. Babonneau, B. Alonso, Chem. Mater. 15 (2003) 4790.
- [34] L.D. Landau, B. Levich, Acta Physicochim. U.R.S.S. 17 (1942) 42.
- [35] I. Strawbridge, P.F. James, J. Non-Cryst. Solids 82 (1986) 366.
- [36] I. Strawbridge, P.F. James, J. Non-Cryst. Solids 86 (1986) 381.
- [37] D.A. Lopez, N.C. Rosero-Navarro, J. Ballarre, A. Durán, M. Aparicio, S. Cere, Surf. Coat. Technol. 202 (2008) 2194.
- [38] M.L. Zheludkevich, R. Serra, M.F. Montemor, I.M. Miranda Salvado, M.G.S. Ferreira, Surf. Coat. Technol. 200 (2006) 3084.
- [39] N.C. Rosero-Navarro, S.A. Pellice, A. Durán, M. Aparicio, Corros. Sci. 50 (2008) 1283.
- [40] M.L. Zheludkevich, D.G. Shchukin, K.A. Yasakau, H. Möhwald, M.G.S. Ferreira, Chem. Mater. 19 (2007) 402.
- [41] S.V. Lamaka, M.L. Zheludkevich, K.A. Yasakau, R. Serra, S.K. Poznyak, M.G.S. Ferreira, Prog. Org. Coat. 58 (2007) 127.